Matlab Simulation of a High Step-Up DC-DC Converter for a Micro grid Application

N.Balaji[1], Dr.S.Satyanarayana[2]

[1]PG Student, Department of EEE, VRS&YRN Engineering College, Chirala,India
[2]Principal, VRS&YRN Engineering College,Chirala,India

Abstract— **A high step-up dc–dc converter for a distributed generation system is proposed in this paper. The concept is composed of two capacitors, two diodes, and one coupled inductor. Two capacitors are charged in parallel, and are discharged in series by the coupled inductor. Thus, high step-up voltage gain can be achieved with an appropriate duty ratio. The voltage stresses on the main switch and output diode are reduced by a passive clamp circuit. Therefore, low resistance R_{DS} (ON) for the main switch can be adopted to reduce conduction loss. In addition, the reverse recovery problem of the diode is alleviated. The operating principle and steady-state analysis of the voltage gain are also discussed in detail. Finally, a MATLAB/Simulink based model is developed with 24v input voltage to obtain 400v output voltage and 400w output power from the proposed converter is simulated in this project.**

Keywords-step-up dc–dc converter, distributed generation system, high step-up voltage gain

I. INTRODUCTION

The distributed generation (DG) systems based on the renewable energy sources have rapidly developed in recent years. These DG systems are powered by micro sources such as fuel cells, photovoltaic (PV) systems, and batteries. Fig. 1.1 shows a PV distributed system in which the solar source is low dc input voltage.
PV sources can also connect in series to obtain sufficient dc voltage for generating ac utility voltage; however, it is difficult to realize a series connection of the PV source without incurring a shadow effect. High step-up dc–dc converters are generally used as the frontend converters to step from low voltage (12–40 V) to high voltage (380–400 V). High step-up dc–dc converters are required to have a large conversion ratio, high efficiency, and small volume.

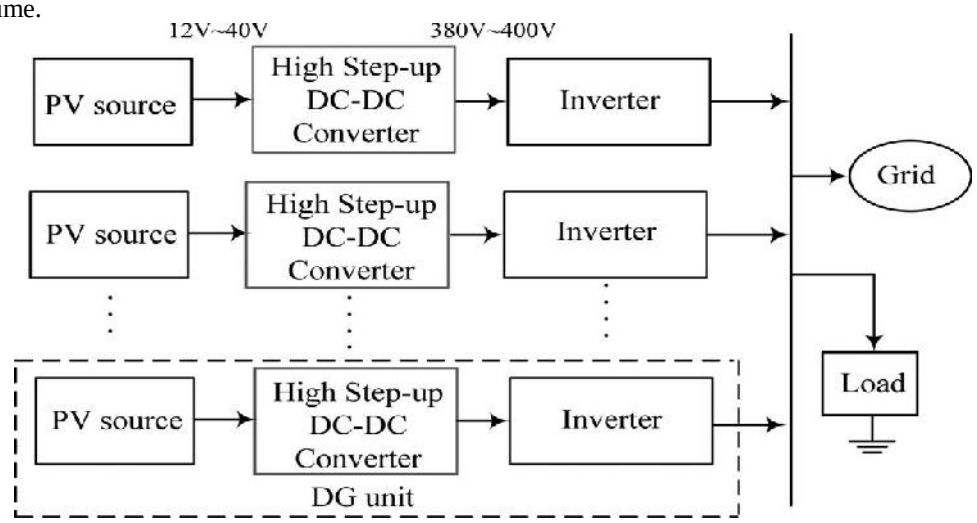

Figure.1.1. PV Distributed System

Distributed energy resource (DER) systems are small-scale power generation technologies (typically in the range of 3 kW to 10,000 kW) used to provide an alternative to or an enhancement of the traditional electric power system. The usual problems with distributed generators are their high costs.

2. PROPOSED CONVERTER

This Proposed Converter has a high efficiency, high step-up voltage gain, and clamp-mode converter. The proposed converter adds two pairs of additional capacitors and diodes to achieve high step-up voltage gain. The coupled inductor is used as both a forward and flyback type; thus, the two capacitors can be charged in parallel and discharged in series via the coupled inductor. The transit current does not flow through the main switch compared with earlier studies. Thus, the proposed converter has low conduction loss. Additionally, this converter allows significant weight and volume reduction compared with other converters. Another benefit is that the voltage stresses on the main switch and output diode are reduced. However, the leakage inductor of the

coupled inductor may cause high power loss and voltage spike. Thus, a passive clamping circuit is needed to recycle the leakage-inductor energy of the coupled inductor and to clamp the voltage across the main switch. The reverse-recovery problems in the diodes are alleviated, and thus, high efficiency can be achieved.

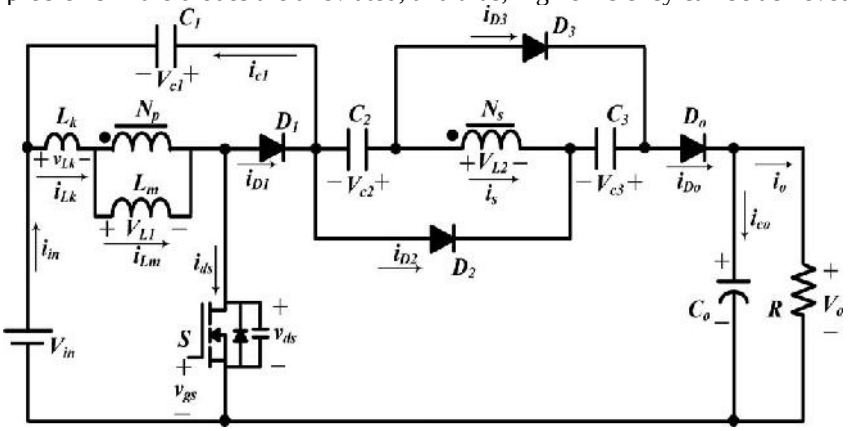

Figure.1. Circuit Configuration of the proposed converter

2.1 Operation

This converter consists of dc input voltage *V*in , power switch *S*, coupled inductors *Np* and *Ns* , one clamp diode *D*1, clamp capacitor *C*1 , two blocking capacitors *C*2 and *C*3 , two blocking diodes *D*2 and *D*3 , output diode *Do* , and output capacitor *Co* . The coupled inductor is modeled as the magnetizing inductor *Lm* and leakage inductor *Lk* .

To simplify the circuit analysis, the following conditions are assumed.

1) Capacitors *C*2 , *C*3 , and *Co* are large enough that *Vc2*, *Vc*3 , and *Vo* are considered to be constant in one switching period.

2) The power MOSFET and diodes are treated as ideal, but the parasitic capacitor of the power switch is considered.

3) The coupling coefficient of coupled inductor *k* is equal to *Lm*/(*Lm*+*Lk*) and the turns ratio of coupled inductor *n* is equal to *Ns* /*Np*.

2.2Continuous-Conduction Mode (CCM) Operation

In CCM operation, there are six operating modes in one switching period of the proposed converter. The operating modes are described as follows.

Mode I [t0 , t1]: During this time interval, *S* is turned on. Diodes *D*1, *D*2, and *D*3 are turned off and *Do* is turned on. The current-flow path is shown in Fig.2. The primary-side current of the coupled inductor *iLk* is increased linearly. The magnetizing inductor *Lm* stores its energy from dc source *V*in. Due to the leakage inductor *Lk* , the secondary-side current of the coupled inductor i_s is decreased linearly. The voltage across the secondary side winding of the coupled inductor *VL* 2 , and blocking voltages *Vc*2 and *Vc*3 are connected in series to charge the output capacitor *Co* and to provide the energy to the load *R*. When the current *is* becomes zero, dc source *V*in begins to charge capacitors *C*2 and *C*3 via the coupled inductor. When *iLk* is equal to *iLm* at *t* = *t*1 , this operating mode ends.

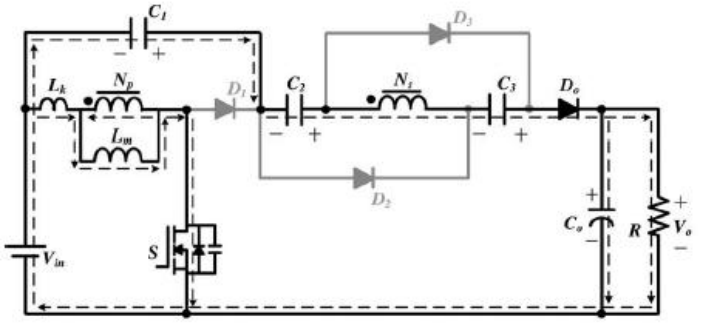

Figure.2. Current flowing path of proposed converter CCM Mode I operation.

Mode II [t1 , t2]: During this time interval, *S* is still turned on. Diodes *D*1 and *Do* are turned off, and *D*2 and *D*3 are turned on. The current-flow path is shown in Fig. 3. The magnetizing inductor *Lm* is stored energy from dc source *V*in . Some of the energy from dc source *V*in transfers to the secondary side of the coupled inductor to charge the capacitors *C*2 and *C*3. Voltages *Vc*2 and *Vc*3 are approximately equal to *nV*in . Output capacitor *Co* provides the energy to load *R*. This operating mode ends when switch *S* is turned off at *t* = *t*2 .

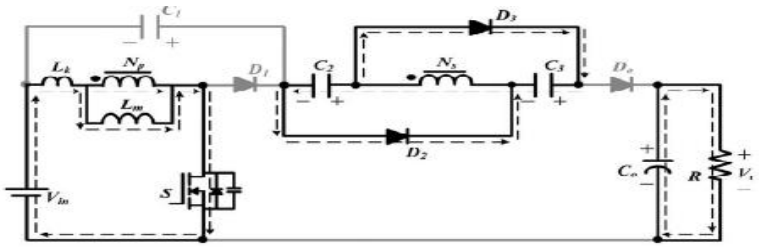

Figure.3. Current flowing path of proposed converter CCM Mode II operation.

Mode III [t2 , t3]: During this time interval, *S* is turned off. Diodes *D*1 and *Do* are turned off, and *D*2 and *D*3 are turned on. The current-flow path is shown in Fig. 4. The energies of leakage inductor *Lk* and magnetizing inductor *Lm* are released to the parasitic capacitor *C*ds of switch *S*. The capacitors *C*2 and *C*3 are still charged by the dc source *V*in via the coupled inductor. The output capacitor *Co* provides energy to load *R*. When the capacitor voltage *V*in+*V*ds is equal to *Vc*1 at $t = t3$, diode *D*1 conducts and this operating mode ends.

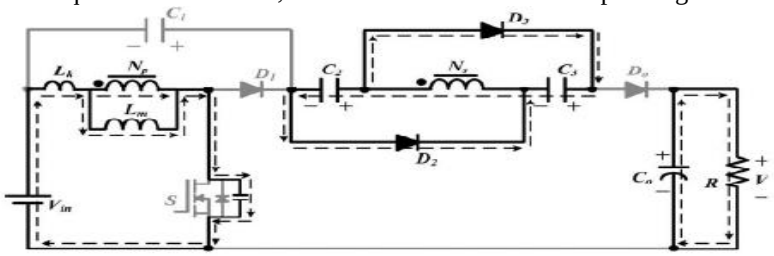

Figure.4. Current flowing path of proposed converter CCM Mode III operation.

Mode IV [t3 , t4]: During this time interval, *S* is turned off. Diodes *D*1 , *D*2 , and *D*3 are turned on and *Do* is turned off. The current-flow path is shown in Fig.5. The energies of leakage inductor *Lk* and magnetizing inductor *Lm* are released to the clamp capacitor *C*1 . Some of the energy stored in *Lm* starts to release to capacitors *C*2 and *C*3 in parallel via the coupled inductor until secondary current *is* equals to zero. Meanwhile, current *iLk* is decreased quickly. Thus, diodes *D*2 and *D*3 are cut off at $t = t4$, and this operating mode ends.

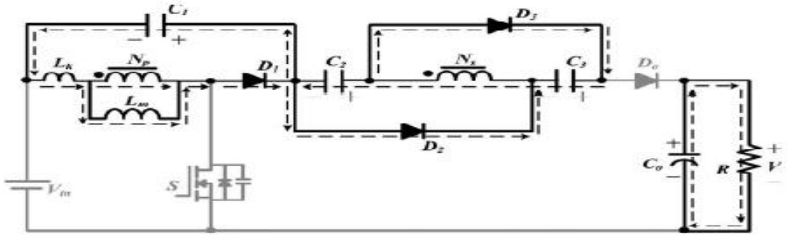

Figure.5. Current flowing path of proposed converter CCM Mode IV operation

***Mode* V [*t*4 , *t*5]:** During this time interval, *S* is turned off. Diodes *D*1 and *Do* are turned on, and *D*2 and *D*3 are turned off. The current-flow path is shown in Fig.6. The energies of leakage inductor *Lk* and magnetizing inductor *Lm* are released to the clamp capacitor *C*1 . The primary and secondary windings of the coupled inductor, dc sources *V*in , and capacitors *C*2 and *C*3 are in series to transfer their energies to the output capacitor *Co* and load *R*. This operating mode ends when capacitor *C*1 starts to discharge at $t = t5$.

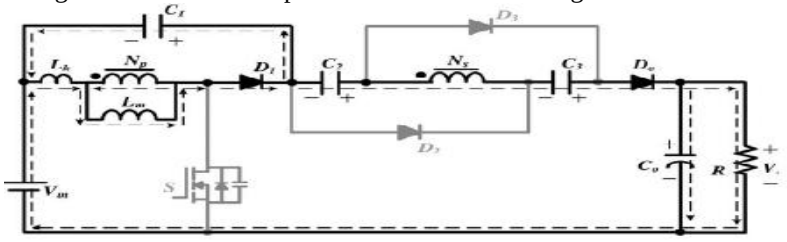

Figure.6. Current flowing path of proposed converter CCM Mode V operation

Mode VI [t5 , t6]: During this time interval, *S* is still turned off. Diodes *D*1 and *Do* are turned on, and *D*2 and *D*3 are turned off. The current-flow path is shown in Fig.7. The primary-side and secondary-side windings of the coupled inductor, dc sources *V*in , and capacitors, *C*1 , *C*2 , and *C*3 , transfer their energies to the output capacitor *Co* and load *R*. This mode ends at $t = t6$ when *S* is turned on at the beginning of the next switching period.

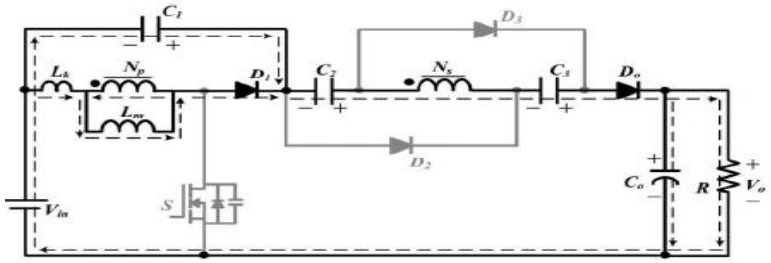

Figure.7. Current flowing path of proposed converter CCM Mode VI operation

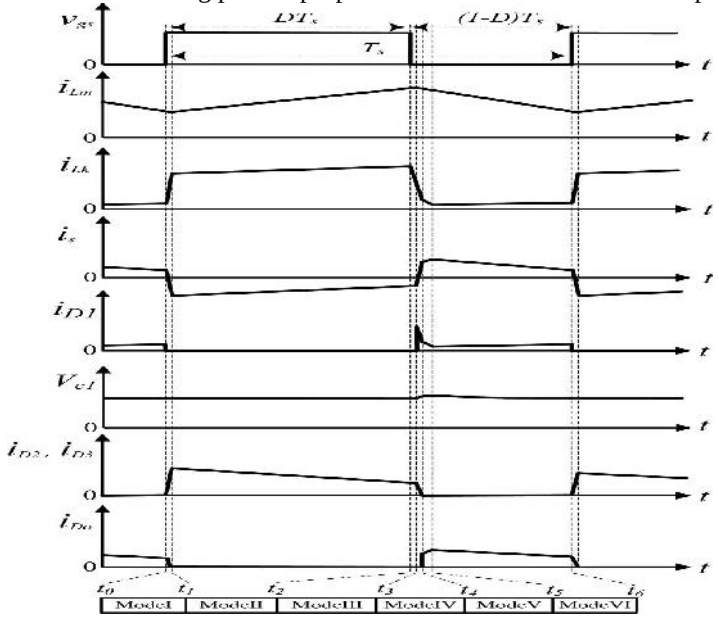

Figure.8.Some typical key waveforms of the proposed converter at CCM operation.

2.4 Dis-Continuous Conduction Mode (DCM) Operation

In order to simplify the analysis for DCM operation, leakage inductor *Lk* of the coupled inductor is neglected. There are three modes in DCM operation. The operating modes are described as follows.

Mode I [t0 , t1]: During this time interval, *S* is turned on. The current-flow path is shown in Fig.9.The part energy of dc source *V*in transfers to magnetizing inductor *Lm*. Thus, *iLm* is increased linearly. The dc source *V*in also transfers another part energy to charge capacitors *C*2 and *C*3 via the coupled inductor. The energy of the output capacitor *Co* is discharged to load *R*. This mode ends when *S* is turned off at $t = t1$.

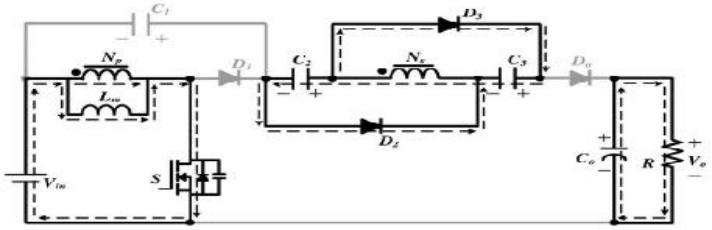

Figure.9. Current flowing path of proposed converter DCM Mode I operation

Mode II [t1 , t2]: During this time interval, *S* is turned off. The current-flow path is shown in Fig.10. The energy of the magnetizing inductor *Lm* is released to the capacitor *C*1. Similarly, capacitors *C*2 and *C*3 are discharged in a series with dc source *V*in and magnetizing inductor *Lm* to the capacitor *Co* and load *R*. This mode ends when the energy stored in *Lm* is depleted at $t = t2$.

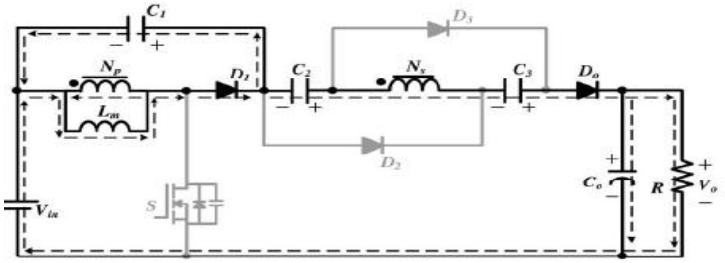

Figure.10. Current flowing path of proposed converter DCM Mode II operation

Mode III [t2 , t3]: During this time interval, *S* remains turned off. The current-flow path is shown in Fig.11. Since the energy stored in *Lm* is depleted, the energy stored in *Co* is discharged to load *R*. This mode ends when *S* is turned on at $t = t3$.

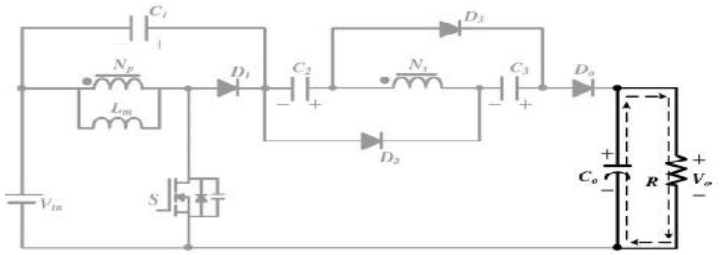

Figure.11. Current flowing path of proposed converter DCM Mode III operation

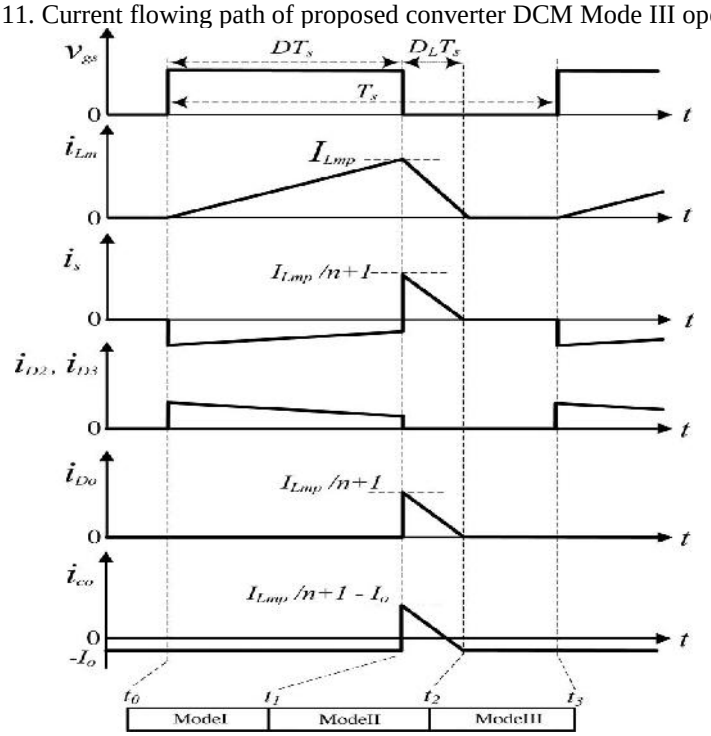

Figure.12.Some typical key waveforms of the proposed converter at DCM operation.

3. STEADY STATE ANALYSIS

3.1.CCM Operation

At modes IV and V, the energy of the leakage inductor *Lk* is released to the clamped capacitor *C*1. According to previous work, the duty cycle of the released energy can be expressed as

$$D_{c1} = \frac{t_{c1}}{T_s} = \frac{2(1-D)}{n+1} \qquad (1)$$

where *Ts* is the switching period, *Dc* 1 is the duty ratio of the switch, and *tc* 1 is the time of modes IV and V. By applying the voltage-second balance principle on *Lm*, the voltage across the capacitor *C*1 can be represented by

$$V_{c1} = \frac{D}{1-D} \cdot V_{\text{in}} \cdot \frac{(1+k)+(1-k)n}{2}. \qquad (2)$$

Since the time durations of modes I, III, and IV are significantly short, only modes II, V, and VI are considered in CCM operation for the steady-state analysis. In the time period of mode II, the following equations can be written based on Fig. 3.

$$v_{L1}^{II} = \frac{L_m}{L_m + L_{k1}} V_{\text{in}} = kV_{\text{in}} \quad (3)$$

$$v_{L2}^{II} = nv_{L1}^{II} = nkV_{\text{in}}. \quad (4)$$

Thus, the voltage across capacitors *C*2 and *C*3 can be written as

$$V_{c2} = V_{c3} = v_{L2}^{II} = nkV_{\text{in}}. \quad (5)$$

During the time duration of modes V and VI, the following equation can be formulated based on Fig.7

$$v_{L2}^{V} = v_{L2}^{VI} = V_{\text{in}} + V_{c1} + V_{c2} + V_{c3} - V_o. \quad (6)$$

Thus, the voltage across the magnetizing inductor *Lm* can be derived as

$$v_{L1}^{V} = v_{L1}^{VI} = \frac{v_{L2}^{VI}}{n} = \frac{V_{\text{in}} + V_{c1} + V_{c2} + V_{c3} - V_o}{n}. \quad (7)$$

Using the volt-second balance principle on *Lm*, the following equation is given:

$$\int_0^{DT_s} v_{L1}^{II} dt + \int_{DT_s}^{T_s} v_{L1}^{VI} dt = 0. \quad (8)$$

Substituting (2), (3), (5), and (7) into (8), the voltage gain is obtained as

$$M_{\text{CCM}} = \frac{1 + nk}{1 - D} + nk + \frac{D}{1 - D} \cdot \frac{(1 - k)(n - 1)}{2}. \quad (9)$$

The ideal voltage gain is written as

$$M_{\text{CCM}} = \frac{1 + n}{1 - D} + n. \quad (10)$$

According to the description of the operating modes, the voltage stresses on the active switch *S* and diodes *D*1 , *D*2 , *D*3 , and *Do* are given as

$$V_{DS} = \frac{1}{1 - D} V_{\text{in}} = \frac{V_o - nV_{\text{in}}}{n + 1} \quad (11)$$

$$V_{D1} = \frac{1}{1 - D} V_{\text{in}} = \frac{V_o - nV_{\text{in}}}{n + 1} \quad (12)$$

$$V_{D2} = V_{D3} = V_{Do} = \frac{n}{1 \quad D} V_{\text{in}} = \frac{n}{n \mid 1} (V_o \quad nV_{\text{in}}). \quad (13)$$

Equations (11)–(13) mean that with the same specifications, the voltage stresses on the main switch and diodes can be adjusted by the turn's ratio of the coupled inductor.

3.2. DCM Operation

In DCM operation, three modes are discussed. The key waveform is shown in Fig. 5. During the time of mode I, the switch *S* is turned on. Thus, the following equations can be formulated based on Fig.9

$$v_{L1}^{I} = V_{\text{in}} \quad (14)$$

$$v_{L2}^{I} = nV_{\text{in}}. \quad (15)$$

The peak value of the magnetizing inductor current is given as

$$I_{Lmp} = \frac{V_{\text{in}}}{L_m} DT_s. \quad (16)$$

Furthermore, the voltage across capacitors *C*2 and *C*3 can be written as

$$V_{c2} = V_{c3} = v_{L2}^{I} = nV_{\text{in}}. \quad (17)$$

In the time interval of mode II, the following equations can be expressed based on Fig.10

$$v_{L1}^{II} = -V_{c1}, \quad (18)$$

$$v_{L2}^{II} = V_{\text{in}} - V_{c1} + V_{c2} + V_{c3} - V_o. \quad (19)$$

During the time of mode III, the following equation can be derived from Fig.2.11

$$v_{L1}^{III} = v_{L2}^{III} = 0. \quad (20)$$

Applying the voltage-second balance principle on *Np* , *Ns* of the coupled inductor, the following equations are given as

$$\int_0^{DT_s} v_{L1}^{I} dt + \int_{DT_s}^{(D+D_L)T_s} v_{L1}^{II} dt + \int_{(D+D_L)T_s}^{T_s} v_{L1}^{III} dt = 0 \tag{21}$$

$$\int_0^{DT_s} v_{L2}^{I} dt + \int_{DT_s}^{(D+D_L)T_s} v_{L2}^{II} dt + \int_{(D+D_L)T_s}^{T_s} v_{L2}^{III} dt = 0. \tag{22}$$

Substituting (14), (15), (17), (18), (19), and (20) into (21) and (22), the voltage gain is obtained as follows:

$$V_{c1} = \frac{D}{D_L} V_{\text{in}} \tag{23}$$

$$V_o = \left[\frac{D}{D_L}(n+1) + (2n+1) \right] V_{\text{in}}. \tag{24}$$

According to (24), the duty cycle *DL* can be derived as

$$D_L = \frac{(1+n)DV_{\text{in}}}{V_o - (1+2n)V_{\text{in}}}. \tag{25}$$

4. SIMULINK MODELS AND RESULTS

The MATLAB/Simulink model of the proposed converter under full load condition (Po=400W) is shown in Fig.4.1. The output voltage 400v obtained is shown in Fig.4.2. The proposed converter is operated in CCM under full-load cindition.The corresponding diode voltage and current waveforms are shown in Fig's.4.3-4.11.Fig.4.3 Output voltage waveform for proposed converter in CCM operation at Vds **is** clamped at appropriately 70v. Fig. 4.5 Output current waveform for proposed converter in CCM operation at IS is clamped at appropriately 10A. Fig's.4.7&4.8 the Output current waveforms of Id2 and Id3 show that capacitors *C*2 and *C*3 are charged in parallel. The diode currentsID2and ID3 are clamped at appropriately 8A. Fig.4.10.Output current waveform for proposed converter in CCM operation at Id0 is clamped at appropriately 10A. Fig.4.11. is Output voltage waveforms for proposed converter in CCM operation at Vd0 shows the voltage stresses of the main switch and diodes.

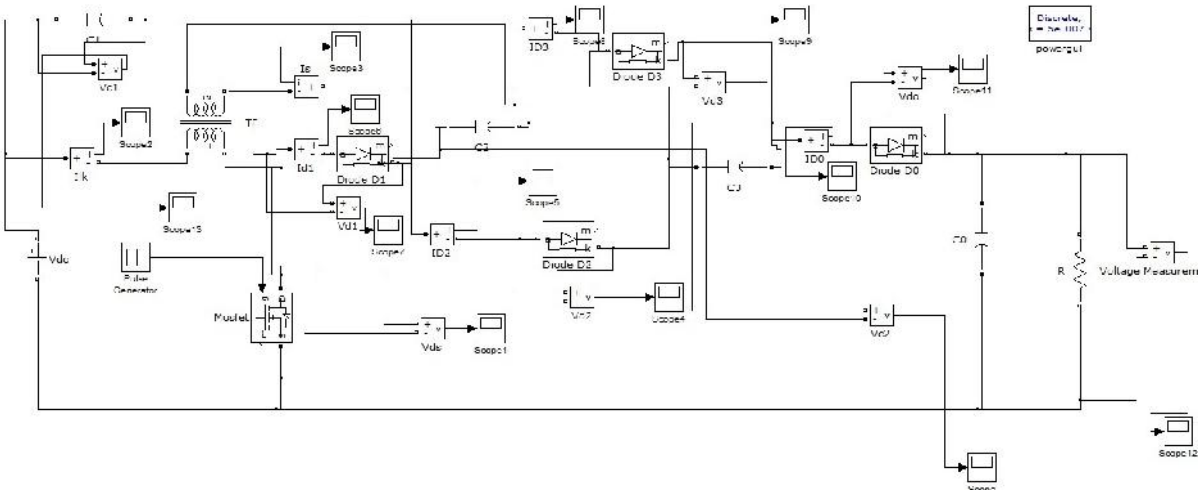

Figure.13 *MATLAB/Simulink Model of the Proposed Converter under Full-Load condition P_o=400W.*

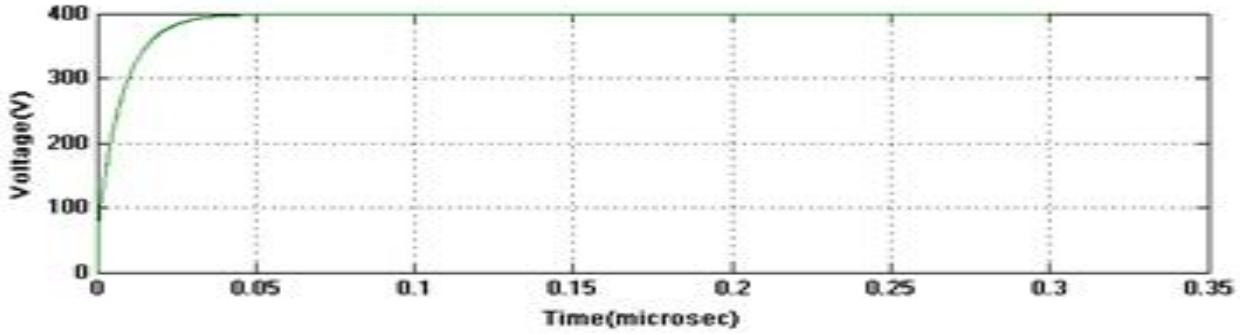

Figure.14**.** *Output voltage waveform for proposed converter in CCM operation*

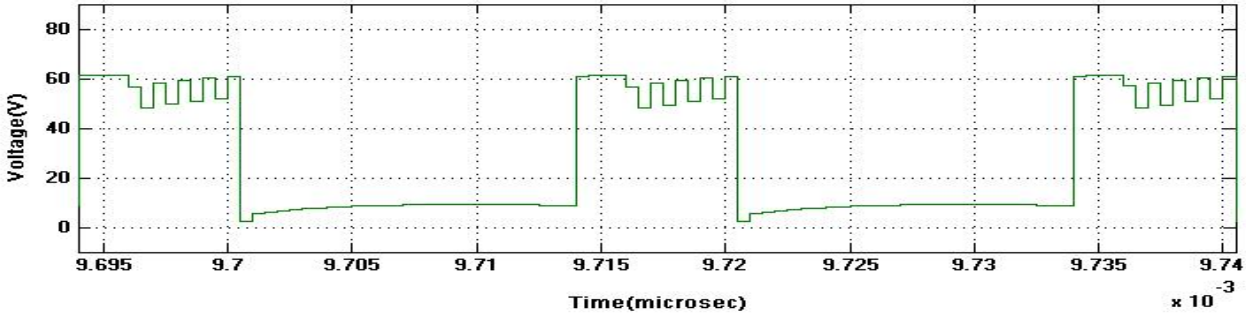

Figure.15. *Output voltage waveform for proposed converter in CCM operation at Vds.*

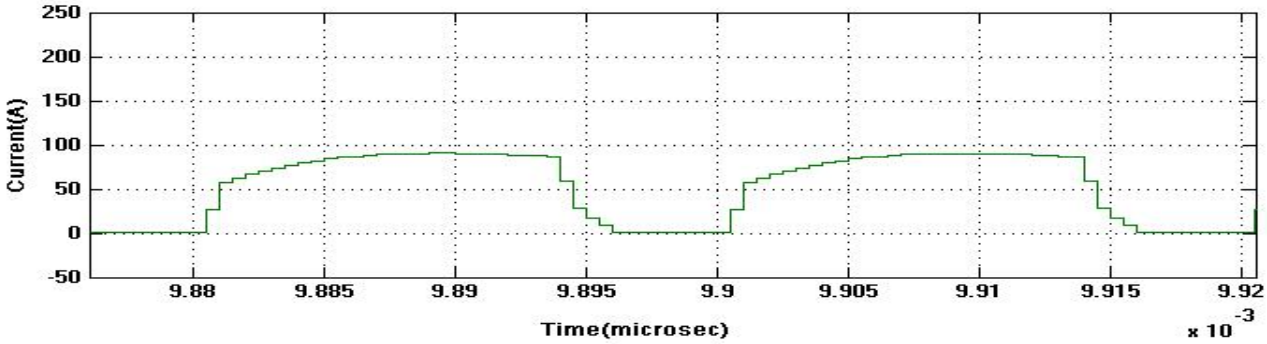

Figure.16. *Output current waveform for proposed converter in CCM operation at Ilk.*

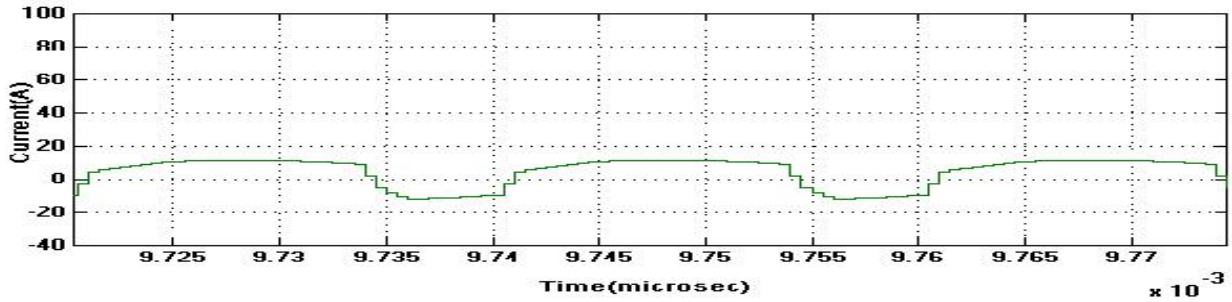

Figur.17 *Output current waveform for proposed converter in CCM operation at IS.*

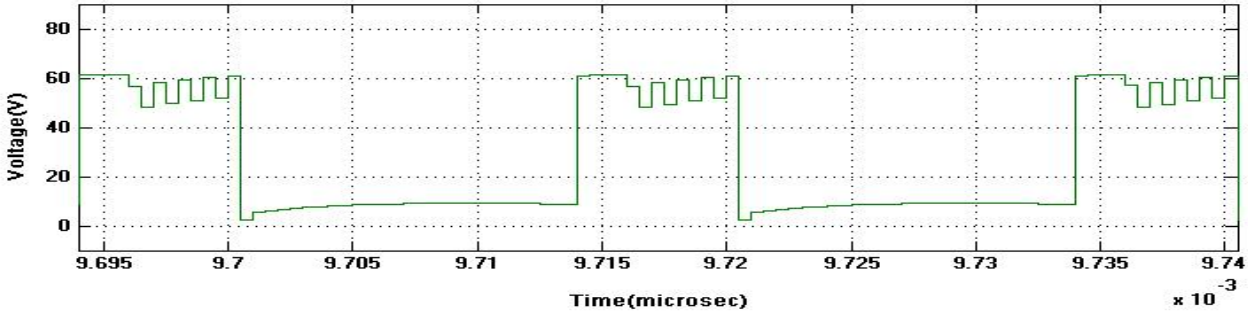

Figure.18**.** *Output voltage waveform for proposed converter in CCM operation at Vds.*

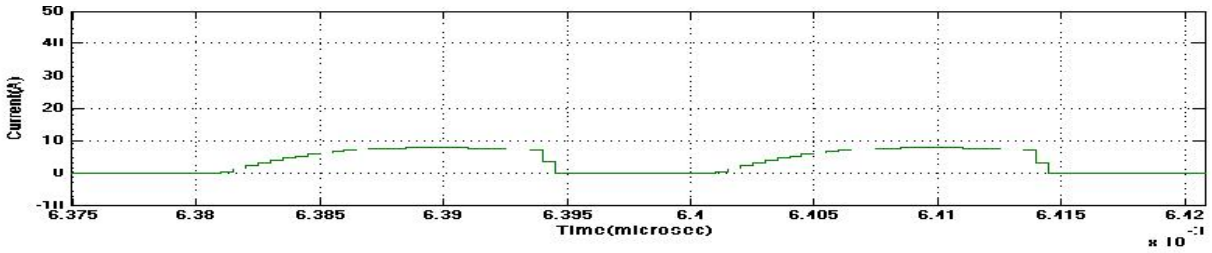

Figure.19 *Output current waveform for proposed converter in CCM operation at Id2.*

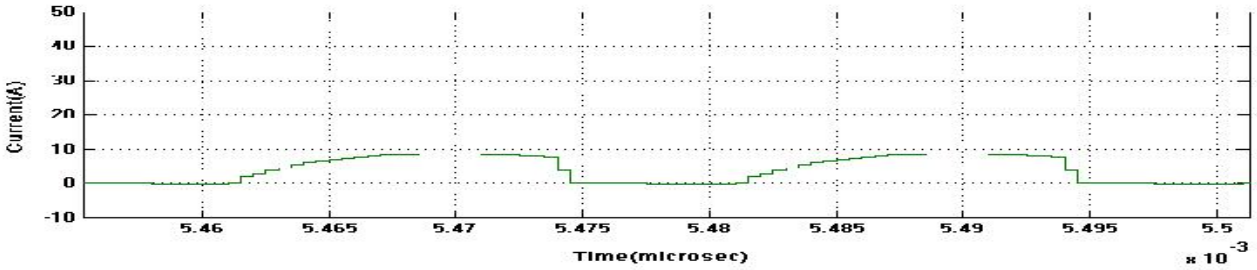

Figure.20 *Output current waveform for proposed converter in CCM operation at Id3.*

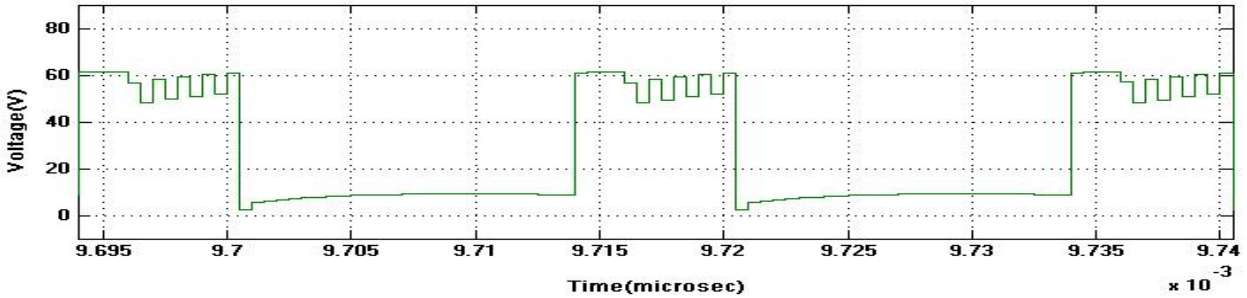

Figure.21. *Output voltage waveform for proposed converter in CCM operation at Vds.*

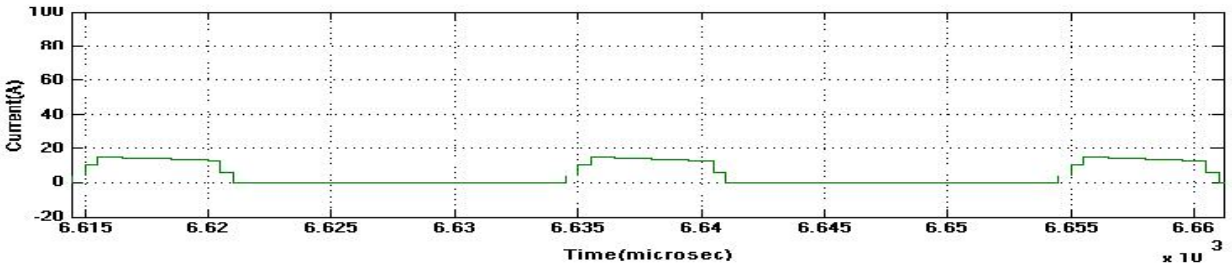

Figure.22. *Output current waveform for proposed converter in CCM operation at Id0.*

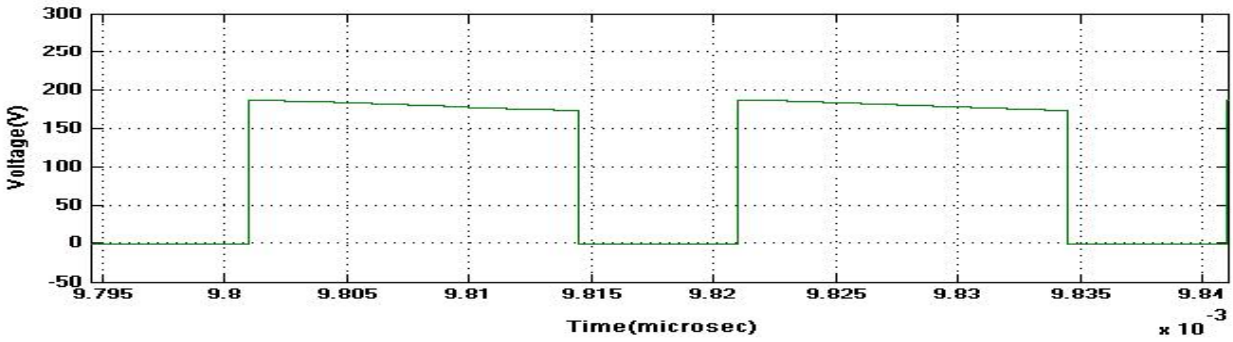

Figure.23. *Output voltage waveforms for proposed converter in CCM operation at Vd0.*

Mode of Operation	**Input Voltage(Vin)**	**Output Voltage(Vo)**
CCM Operation	24	400
DCM Operation	24	500

Table.1.Comparison Table of the proposed converter

5. CONCLUSION

A step-up dc–dc converter is designed and Simulated in this project. By using the capacitor charged in parallel and discharged in a series by the coupled inductor, a high step-up voltage gain is achieved. The steady-state analysis of voltage gain is discussed in detail. Simulation results confirm that high step-up voltage gain is achieved. Moreover, the proposed converter has simple structure. It is suitable for renewable energy systems in microgrid applications.

REFERENCES

[1] Y. Li and Y. W. Li, "Decoupled power control for an inverter based low voltage microgrid in autonomous operation," in *Proc. IEEE Int. Power Electron. Motion Control Conf. (IPEMC)*, 2009, pp. 2490–2496.

[2] Y. Li, D. M. Vilathgamuwa, and P. H. Loh, "Design, analysis, and real-time testing of a controller for Multibus microgrid system," *IEEE Trans. Power Electron.*, vol. 19, no. 5, pp. 1195–1204, Jul. 2004.

[3] C. L. Chen, Y. W, J. S. Lai, Y. S. Lee, and D. Martin, "Design of parallel inverters for smooth mode transfer microgrid applications," *IEEE Trans. Power Electron.*, vol. 25, no. 1, pp. 6–15, Jan. 2010.

[4] A. Timbus, M. Liserre, R. Teodorescu, P. Rodriguez, and F. Blaabjerg, "Evaluation of current controllers for distributed power generation systems," *IEEE Trans. Power Electron*., vol. 24, no. 3, pp. 654–664, Mar. 2009.

[5] Y. A.-R. I. Mohamed and E. F. El Saadany, "Hybrid variable-structure control with evolutionary optimum tuning algorithm for fast grid-voltage regulation using inverter-based distributed generation," *IEEE Trans Power Electron*, vol. 23, no. 3, pp. 1334–1341, May 2008.

[6] Y. A.-R. I. Mohamed and E. F. El Saadany, "Adaptive decentralized droop controller to preserve power sharing stability of paralleled inverters in distributed generation microgrids," *IEEE Trans. Power Electron.*,vol. 23, no. 6, pp. 2806–2816, Nov. 2008.

[7] Y. W. Li and C. -N. Kao, "An accurate power control strategy for power electronics- interfaced distributed generation units operating in a low voltage multibus microgrid," *IEEE Trans. Power Electron.*, vol. 24, n 12, pp. 2977–2988, Dec. 2009.

[8] H. Karimi, A. Yazdani, and R. Iravani, "Negative-sequence current injection for fast islanding detection of a distributed resource unit," *IEEE Trans. Power Electron.*, vol. 23, no. 1, pp. 298–307, Jan. 2008.

[9] T. Shimizu, K.Wada, andN.Nakamura, "Flyback-type single-phase utility interactive inverter with power pulsation decoupling on the dc input for an ac photovoltaic module system," *IEEE Trans. Power Electron* vol. 21, no. 5, pp. 1264–1272, Sep. 2006.

[10] L. Palma, M. H. Todorovic, and P. Enjeti, "A high gain transformer less DC–DC converter for fuel-cell applications," in *Proc. IEEE Power Electron. Spec. Conf. (PESC)*, 2005, pp. 2514–2520.